Encyclopedia of Microfluidics and Nanofluidics
DOI 10.1007/978-3-642-27758-0_1155-2

Optical Coherence Tomography and Optical Doppler Tomography

Zhongping Chen*
Department of Biomedical Engineering, University of California, Irvine, CA, USA

Synonyms

Doppler OCT; Optical coherence imaging; Optical Doppler tomography (ODT); Optical Doppler velocimetry

Definition

Optical coherence tomography (OCT) is an interferometric, noninvasive, noncontact optical tomographic imaging modality based on coherence-domain optical technology [1–6]. OCT uses the short coherence length of a broadband light source to perform cross-sectional imaging with micrometer-scale axial and lateral resolutions. Optical Doppler tomography (ODT), also named Doppler OCT, combines the Doppler principle with OCT to obtain simultaneously high-resolution tomographic images of structure and flow velocity of scattering samples [7, 8].

Overview and Basic Methodology

Optical Coherence Tomography

OCT is a recently developed interferometric imaging modality that uses short coherence length of broadband light sources to perform micrometer-scale, cross-sectional imaging of biological tissue and other sample. Variations in sample scattering due to inhomogeneities in the optical index of refraction provide imaging contrast. OCT is analogous to ultrasound imaging except that it uses light instead of sound wave. The short coherence length of the broadband light source makes it possible to achieve spatial resolution one or two orders of magnitude better than what can be achieved with ultrasound. OCT was initially developed for imaging biological tissue for medical applications [2]. Since then, OCT has been used for imaging and quantifying biomaterials, microchannels, and nanostructures [3, 5, 8].

There are two basic implementations of OCT, time domain OCT (TD-OCT) and Fourier domain OCT (FD-OCT). TD-OCT is based on a Michelson interferometer with a broadband light source (Fig. 1). Light from a broadband partial coherent source is incident on the beam splitter and splits equally between reference and target arms of the interferometer. Light backscattered from the turbid sample recombines with light reflected from the reference arm and forms interference fringes. High axial spatial resolution is possible because interference fringes are observed only when the path length differences between the sample arm and reference arm are within the coherence length of the source. Axial scans are performed by scanning the reference arm, and lateral scans are performed by scanning the sample beam. A two-dimensional, cross-sectional image is formed by performing an

*Email: z2chen@uci.edu

DOI 10.1007/978-3-642-27758-0_1155-2

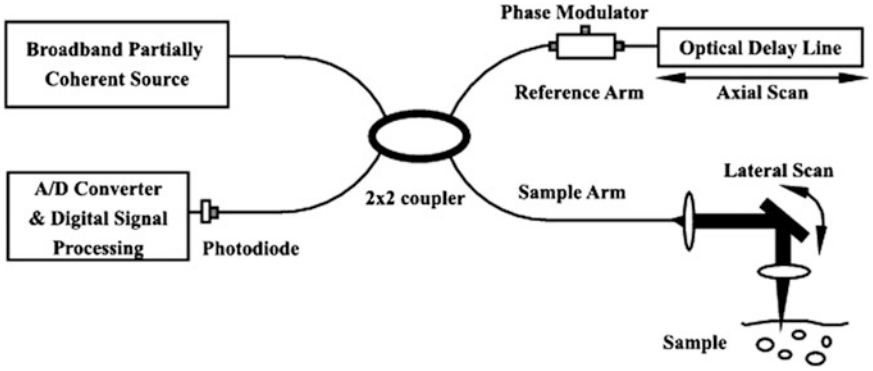

Fig. 1 Schematic of a time domain OCT system consisting of a fiber-based Michelson interferometer with a partially coherent light source

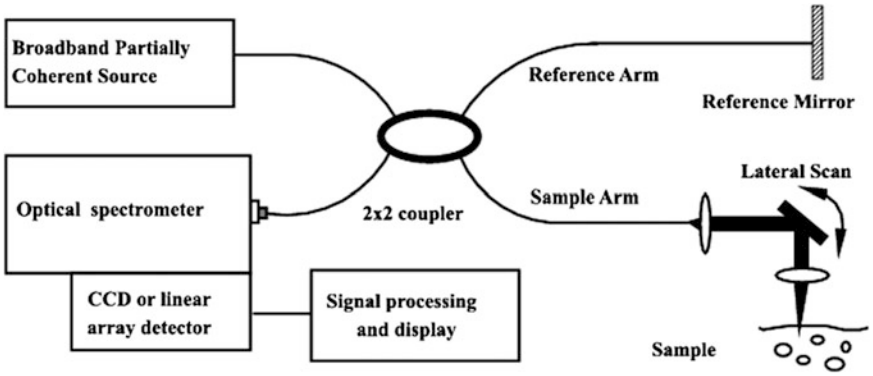

Fig. 2 Schematic of a spectrometer-based Fourier domain OCT system

axial scan followed by a lateral scan. Axial resolution is determined by the coherence length of the source, and lateral resolution is determined by the numerical aperture of the focusing lens [1–6].

Fourier domain OCT measures interference fringes in the spectral separated domain either by a spectrometer with a high-speed line-scan camera (Fig. 2) or a swept laser source-based system that uses a single detector [3, 6, 8]. Modulation of the interference fringe intensity in the spectral domain is used to determine the location of all scattering objects along the beam propagation direction by a Fourier transformation without scanning of the reference arm. FD-OCT has the advantages of high sensitivity and fast imaging speed. The significant increase in imaging speed and sensitivity of FD-OCT makes it possible to acquire three-dimensional OCT images with high spatial resolution.

An example of OCT applications in microfluidics is the investigation of laminar dispersion in a serpentine microchannel with a Y-shape inlet (Fig. 3). Transient two-fluid mixing in microfluidic devices can be clearly observed (Fig. 4) [9].

Optical Doppler Tomography

ODT combines the Doppler principle with OCT to obtain high-resolution tomographic images of static and moving constituents simultaneously in scattering samples [5, 8, 10, 11]. When light backscattered from a moving particle interferes with the reference beam, a Doppler frequency shift f_D occurs in the interference fringe:

DOI 10.1007/978-3-642-27758-0_1155-2

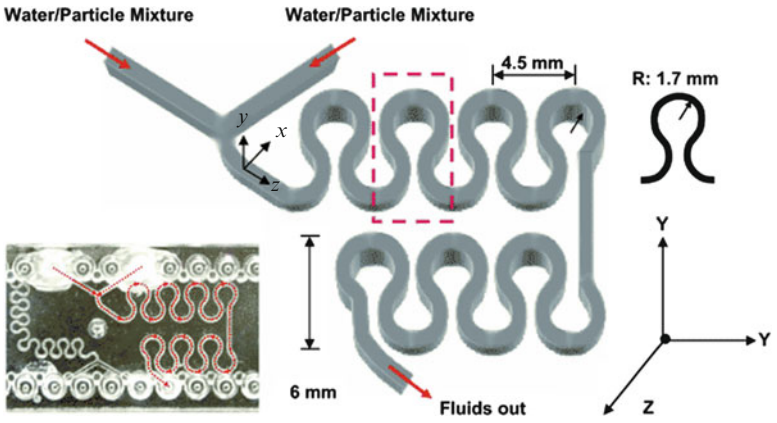

Fig. 3 Picture and schematic of a meandering square microchannel made of cyclo-olefin copolymer. It has a Y branch at the beginning and the dimension of cross section between confluence and outlet is 600 × 600 μm. The radius of curvature *R* is 1.7 mm. The *red dotted line* indicates area of interest

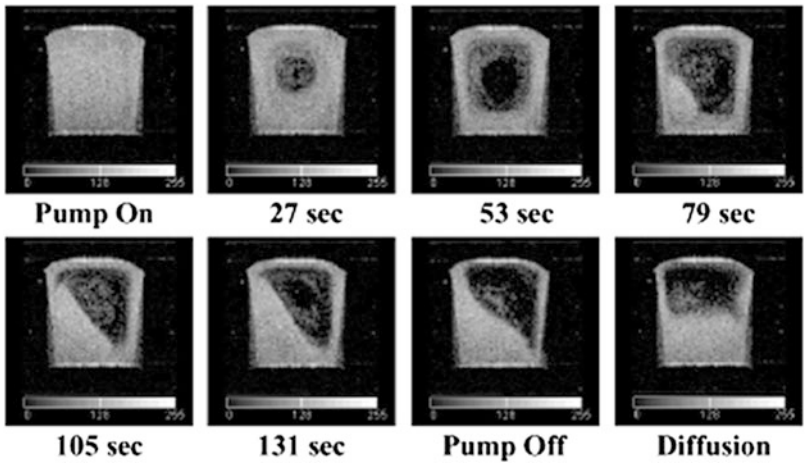

Fig. 4 OCT images of transient two-fluid mixing in a meandering square microchannel as shown in Fig. 3. Initially, the entire channel was filled with a particle/water mixture, and the dual-syringe pump (one with the particle/water mixture, and the other with water only) was turned off. As soon as the pump was turned on with a programmed flow rate, OCT images were acquired at 1 frame per second. When the initial mixing was stabilized and reached a dynamic steady state, the pump was turned off again. At the dynamic steady state, sedimentation was observed macroscopically. Stratification between the water and particle/water mixture was developed, and a clear interface was observed in the transverse plane. Secondary flow at the dynamic steady state is clearly visible. Finally, the concentration reached a static steady state where scattering particles occupied the lower half cross section which resulted from sedimentation

$$f_{\mathrm{D}} = \frac{1}{2\pi}(k_s - k_i) \bullet v, \tag{1}$$

where k_i and k_s are wave vectors of incoming and scattered light, respectively, and v is the velocity vector of the moving particle (Fig. 5). Since ODT measures the backscattered light, assuming the angle between flow and sampling beam is θ, the Doppler shift equation is simplified to:

DOI 10.1007/978-3-642-27758-0_1155-2

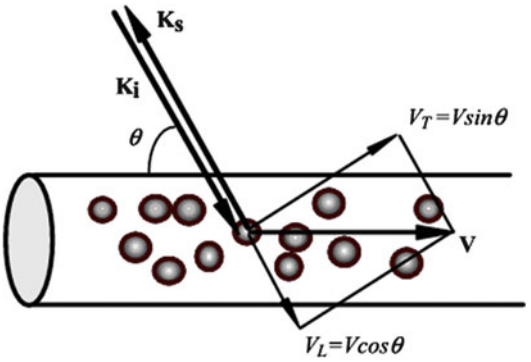

Fig. 5 Schematic of flow direction and probe beam angle in ODT

$$f_{\mathrm{D}} = \frac{2V\cos\theta}{\lambda_0}, \tag{2}$$

where λ_0 is the vacuum center wavelength of the light source. Therefore, measurement of Doppler shift of the backscattered light allows quantification of flow velocity of scattering particles.

The optical system of ODT is similar to that of OCT. The primary difference is in signal processing. The first two-dimensional in vivo ODT imaging was reported using the spectrogram method [10, 11]. The spectrogram method uses a short time fast Fourier transformation or wavelet transformation to determine the power spectrum of the measured fringe signal [10, 11]. Although spectrogram methods allow simultaneous imaging of in vivo tissue structure and flow velocity, the velocity sensitivity is limited for high-speed imaging. Phase-resolved Doppler OCT was developed to overcome these limitations [12]. This method uses the phase change between sequential A-line scans for velocity image reconstruction [8, 12]. Phase-resolved Doppler OCT decouples spatial resolution and velocity sensitivity in flow images and increases imaging speed by more than two orders of magnitude without compromising spatial resolution and velocity sensitivity [8, 12].

In phase-resolved ODT, the phase information of the fringe signal can be determined from the complex analytical signal $\widetilde{\Gamma}(t)$, which is determined through analytic continuation of the measured interference fringe function, $\Gamma(t)$, using a Hilbert transformation [8]:

$$\widetilde{\Gamma}(t) = \Gamma(t) + \frac{i}{\pi} P \int_{-\infty}^{\infty} \frac{\Gamma(\tau)}{\tau - t} \mathrm{d}\tau = A(t) e^{i\phi(t)}, \tag{3}$$

where P denotes the Cauchy principle value, i is the complex number, and $A(t)$ and $\phi(t)$ are amplitude and phase term of $\widetilde{\Gamma}(t)$, respectively. Because the interference signal $\Gamma(t)$ is quasi-monochromatic, the complex analytical signal can be determined by:

$$\widetilde{\Gamma}(t) = 2\int_0^{\infty}\int_0^{\tau} \Gamma(t')\exp(-2\pi i v t')\mathrm{d}t'\exp(2\pi i v t)\mathrm{d}v,$$

where τ is the time duration of the fringe signal in each axial scan.

DOI 10.1007/978-3-642-27758-0_1155-2

The Doppler frequency shift f_n at nth pixel in the axial direction can be determined from the average phase shift between sequential A-scans. This can be accomplished by calculating the phase change of sequential scans from the individual analytical fringe signal [8]:

$$f_n = \frac{\Delta\phi}{2\pi T} = \frac{1}{2\pi T} \sum_{m=(n-1)M}^{nM} \sum_{j=1}^{N} \left[\tan^{-1}\left(\frac{\mathrm{Im}\widetilde{\Gamma}_{j+1}(t_m)}{\mathrm{Re}\widetilde{\Gamma}_{j+1}(t_m)} \right) - \tan^{-1}\left(\frac{\mathrm{Im}\widetilde{\Gamma}_{j}(t_m)}{\mathrm{Re}\widetilde{\Gamma}_{j}(t_m)} \right) \right]. \tag{4}$$

Alternatively, the phase change can also be calculated by the cross-correlation method [8]:

$$f_n = \frac{1}{2\pi T} \tan^{-1}\left(\frac{\mathrm{Im}\left[\sum_{m=(n-1)M}^{nM} \sum_{j=1}^{N} \widetilde{\Gamma}_j(t_m)\widetilde{\Gamma}^*_{j+1}(t_m) \right]}{\mathrm{Re}\left[\sum_{m=(n-1)M}^{nM} \sum_{j=1}^{N} \widetilde{\Gamma}_j(t_m)\widetilde{\Gamma}^*_{j+1}(t_m) \right]} \right). \tag{5}$$

where $\widetilde{\Gamma}_j(t_m)$ and $\widetilde{\Gamma}^*_j(t_m)$ are the complex signals at axial time t_m corresponding to the jth A-scan and its respective conjugate $\widetilde{\Gamma}_{j+1}(t_m)$ and $\widetilde{\Gamma}^*_{j+1}(t_m)$ are the complex signals at axial time t_m corresponding to the next A-scan and its respective conjugate, M is an even number that denotes the window size in the axial direction for each pixel, N is the number of sequential scans used to calculate the cross-correlation, and T is the time duration between A-scans. Because T is much longer than the pixel time window within each scan used in the spectrogram method, high-velocity sensitivity can be achieved.

In addition to the local velocity information, the standard deviation of the Doppler spectrum gives the variance of local velocity and can be determined from the measured analytical fringe signal [8]:

$$\sigma^2 = \frac{1}{(2\pi T)^2} \times \left(1 - \frac{\sum_{m=(n-1)M}^{nM} \sum_{j=1}^{N} \widetilde{\Gamma}_j(t_m)\widetilde{\Gamma}^*_{j+1}(t_m)}{\frac{1}{2}\sum_{m=(n-1)M}^{nM} \sum_{j=1}^{N} \left[\widetilde{\Gamma}_j(t_m)\widetilde{\Gamma}^*_j(t_m) + \widetilde{\Gamma}_{j+1}(t_m)\widetilde{\Gamma}^*_{j+1}(t_m) \right]} \right), \tag{6}$$

The σ value depends on the flow velocity distribution. Variations in flow velocity will broaden the Doppler frequency spectrum and result in a large σ value. Thus, the Doppler variance image can be an indicator of flow variations and can be used to study flow turbulences. In addition, standard deviation imaging can also be used to determine the transverse flow velocity [8].

The significant increase in velocity sensitivity of phase-resolved ODT makes it possible to image in vivo tissue microcirculation. Recently, the development of FD-OCT has significantly increased imaging speed and sensitivity. Combination of FD-OCT with the phase-resolved method has been demonstrated by a number of groups [8]. Because the dynamic range of the phase-resolved ODT depends on the speed of the line scans, Fourier domain ODT has an advantage over the time domain method in terms of imaging speed and velocity dynamic range [8].

ODT can provide cross-sectional imaging of channel geometry and flow velocity simultaneously. It has been used to measure osmotic mobility, quantify size of the scattering particle, and study flow dynamics of microfluidic devices of different materials, geometry, junction, and surface treatment [8, 13]. ODT has also been used to image and quantify two-phase flow and flow mixing [8, 9, 14, 15].

DOI 10.1007/978-3-642-27758-0_1155-2

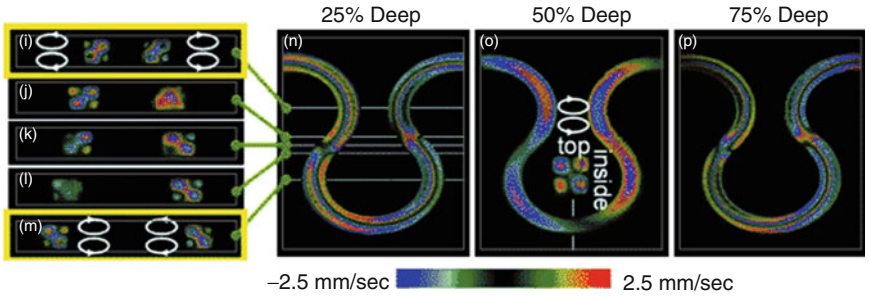

Fig. 6 ODT images of secondary flow in a meandering square microchannel as shown in Fig. 3. The measured z components of the flow velocity $V_z(x,y,z)$ in the area of interest was projected into different cross-sectional planes, where the z axis is perpendicular to the microchannel plane (x-y plane) and along the direction of the ODT probe beam. (**i**–**m**) cross-sectional mapping of secondary flow velocity $V_z(x,z)$ at different y positions. (**n**–**p**) cross-sectional mapping of secondary flow velocity $V_z(x,y)$ at different z positions (depth). *Inset* (**o**) is a cross-sectional mapping of secondary flow velocity $V_z(y,z)$ at the center of the channel as indicated by the *white line*

An example of ODT applications to simultaneously image and quantify the secondary flow and mixing pattern in microchannels is shown in Fig. 6 [15]. Aqueous suspension of polystyrene beads with a diameter of 0.2 μm and concentration of 20.5 mg/cc was injected into both inlets of the *Y* branch device of a meandering microchannel with a square cross section as shown in Fig. 3. The probe beam of the FD-ODT was adjusted to be approximately perpendicular to the plane of the microchannel (x-y plane). Because primary flow is in the x-y plane and the probe beam is in the z direction, ODT is not sensitive to the primary flow in such a probe configuration. Consequently, only the secondary flow will contribute to the Doppler signal. The z-component of the secondary flow velocity $V_z(x,y,z)$ was imaged and quantified with FD-ODT. Figure 6i–m shows cross-sectional mapping of secondary flow velocity $V_z(x,z)$ in the x-z plane at different y positions as indicated. The velocity field at x-z plane shows a pair of counterrotating vortices. Since the curvature is alternating, the rotational direction of the vortices is also alternating as shown by comparing Fig. 6i–m. Figure 6n–p shows cross-sectional mapping of secondary flow velocity $V_z(x,y)$ at different z positions. Alternating flow direction of the secondary flow at different depth in the x-y plane can be clearly visualized. The inset in Fig. 6o is a cross-sectional mapping of secondary flow velocity $V_z(y,z)$ in the y-z plane at the center of the channel as indicated by the white line. The velocity field at the y-z plane shows a pair of counterrotating vortices. This result clearly demonstrates that ODT can be used to image and quantify secondary flow [15].

Future Directions for Research

OCT and ODT are rapidly developing technologies with many potential applications for imaging and quantifying microfluidic flow dynamics in BioMEMS devices. New developments in all components of an OCT/ODT system, including light sources, detection electronics, and phase-resolved processing algorithms can further increase imaging speed and sensitivity. Given its noninvasive and noncontact nature and exceptionally high spatial resolution and velocity sensitivity, OCT/ODT will be a powerful metrology tool for investigating complex flow dynamics in various BioMEMS devices that involve microfluidics.

DOI 10.1007/978-3-642-27758-0_1155-2

Cross-References

- ▶ AC Electro-Osmotic Flow
- ▶ Active Mixer
- ▶ Micro-PIV-Based Diffusometry
- ▶ Velocity Sensors

References

1. Huang D et al (1991) Optical coherence tomography. Science 254(5035):1178–1181
2. Bouma BE, Tearney GJ (2002) Handbook of optical coherence tomography. Dekker, New York
3. Fercher AF, Hizenberger CK (2002) Optical coherence tomography. In: Wolf E (ed) Progress in optics. Elsevier, North Holland, p 215
4. Chen Z (2003) Functional optical coherence tomography. In: Hwang NHC, Woo SLY (eds) Frontiers in biomedical engineering. Kluwer Academic/Plenum, New York, pp 345–364
5. Chen Z (2004) Tomography and optical imaging. In: Guenther BD (ed) Encyclopedia of modern optics. Elsevier, New York
6. Brezinski ME (2006) Optical coherence tomography. Elsevier, New York
7. Chen Z et al (1997) Optical Doppler tomographic imaging of fluid flow velocity in highly scattering media. Opt Lett 22:64–66
8. Chen Z (2004) Optical Doppler tomography. In: Tuchin VV (ed) Coherent-domain optical methods for biomedical diagnostics, environmental and material science. Kluwer Academic, Boston, pp 315–340
9. Ahn YC et al (2005) Investigation of laminar dispersion with optical coherence tomography and optical Doppler tomography. Opt Express 13:8164–8171
10. Chen Z et al (1997) Noninvasive imaging of in vivo blood flow velocity using optical Doppler tomography. Opt Lett 22:1119–1121
11. Izatt JA et al (1997) In vivo bidirectional color Doppler flow imaging of picoliter blood volumes using optical coherence tomography. Opt Lett 22:1439–1441
12. Zhao Y et al (2000) Phase-resolved optical coherence tomography and optical Doppler tomography for imaging blood flow in human skin with fast scanning speed and high velocity sensitivity. Opt Lett 25:114–116
13. Wang RK (2004) High-resolution visualization of fluid dynamics with Doppler optical coherence tomography. Meas Sci Technol 15:725–733
14. Ahn YC, Jung W, Chen Z (2006) Tubid two-phase slog flow in a microtube simultaneous visualization of structure and velocity field. Appl Phys Lett 89:064109
15. Ahn YC, Jung W, Chen Z (2008) Optical sectioning for microfluidics: secondary flow and mixing in a meandering microchannel. Lab Chip 8:125–133